Tuijin Jishu/Journal of Propulsion Technology
ISSN: 1001-4055
Vol. 47 No. 02 (2026)

Coordinated EV Charging and Discharging Strategy Using a Mamdani MIMO Fuzzy Controller: Application to the Onitsha 11-kV Network

Onyemenam John O.[1*], Olulope Paul K.[2], Adebiyi Marion[3], Yusuf Isaac O.[4], Ariba Folashade O.[5], Dada Theophilus[6]

[1,4,6]Department of Electrical and Information Engineering Landmark University SDG 9 (Industry, Innovation and Discoveries), Omu-Aran, Kwara State, Nigeria)
[2]Department of Electrical and Electronics Engineering, Ekiti State University
[3]Department of Computer Science, Nile University of Nigeria
[5]Department of Electrical and Electronic Engineering, Federal University of Technology and Environmental Sciences, Iyin-Ekiti, Ekiti State, Nigeria

Abstract: Modern electricity distribution networks are facing serious operating difficulties as a result of the explosive proliferation of electric vehicles (EVs), especially in areas like Nigeria's Onitsha distribution network that have little grid flexibility. Severe voltage imbalance, frequency aberrations, and higher power losses can result from uncoordinated grid-to-vehicle (G2V) charging and vehicle-to-grid (V2G) discharging. In order to effectively coordinate EV charging and discharging while maintaining grid stability, this work creates a Multi-Input Multi-Output (MIMO) Mamdani fuzzy logic controller. The controller generates two outputs: charging rate and a quantitative grid stability index by integrating four real-time indicators: State of Charge (SOC), Time Remaining (TR), grid frequency, and grid voltage. To capture expert operating logic, eighty-one fuzzy rules were created, allowing for the simultaneous optimization of charging performance and stability support. The Onitsha 11 kV network model, comprising 29 load centers and two injection substations, was used to validate the controller's performance across five critical operating scenarios ranging from charging-priority to grid-critical and rapid-discharging conditions. Comparative evaluation with a conventional PI controller and a DISO fuzzy controller showed that the MIMO controller consistently achieved superior grid stability indices (0.826– 0.846 in normal conditions) and provided effective protective behavior during grid-critical states by entering safe idle mode. Frequency deviation was also reduced by up to 22% compared to baseline controllers. Statistical significance tests further confirmed the superiority of the MIMO controller in specific pairwise comparisons. Overall, the proposed MIMO Mamdani controller presents a robust, adaptive, and intelligent solution for coordinated EV integration in weak distribution networks.

Keywords: MIMO fuzzy controller, Onitsha distribution network, EV charging, vehicle-to-grid, fast charging.

1. Introduction

Electric vehicles have emerged as a possible alternative in this transition. In recent years, numerous countries have created extensive programs to boost the use of electric vehicles. For example, China has established about 2,000 charging stations and 13,000 charging piles as part of its "ten cities, thousand vehicles" initiative [1]. However, as the number of electric vehicles develops, more batteries connect to the grid, increasing the pressure on local power utilities and their charging infrastructure. Power grids encounter overload and other unforeseen effects in the absence of coordinated charging and discharging techniques because charging and discharging behaviors cannot be appropriately scheduled [2]-[3]. Phase imbalance, voltage drop, harmonic distortion, and higher power losses are some of the issues caused by uncontrolled charging and discharging. Removing these passive impacts requires scheduling charging behaviors. According to Qian et al. [2], there are peak and off-peak times for power consumption in each given area. According to Tang et al. [4], an intelligent charging strategy must schedule the charging load for off-peak times and determine when an electric car needs to be charged. Additionally, some electric vehicles' excess energy can be returned to charging stations to satisfy the demands of other vehicles that need to be charged, lessening the burden on the stations. When solving the charging issue, this creates a mobile social network between electric vehicles and charging stations [5]–[6]. While current fuzzy logic implementations usually maximize single objectives like cost or charging speed without specific stability monitoring, conventional

proportional-integral controllers are unable to react to sudden changes in grid frequency and voltage [7]–[8]. Additionally, machine learning-based consistency verification and thorough statistical significance assessment are lacking in validation procedures for intelligent controllers, which mostly rely on limited scenario testing. Additionally, real-time grid indications are not incorporated into traditional PI and simplified fuzzy controllers, and thus lack multi-objective capacity. In order to simultaneously maximize charging and grid stability, this study uses a MIMO Mamdani fuzzy inference system (FIS).

2. Network model

The Onitsha distribution network, an actual Nigerian power system operating in Anambra State, is managed by the Enugu Electricity Distribution Company. This network supplies 29 load centers with two injection substations located in Awada and GCM. With line requirements of 0.4Ω/km resistance and 0.3Ω/km reactance, each substation is connected to thirteen distribution transformers rated at 11kV/415V. The load center specifications, which include apparent power requirements, active power demands, and power factors gathered from Enugu Electricity Distribution Company records, are shown in Table 1. Figure 1 shows the relationships between substations, transmission lines, and load centers in the Onitsha distribution network's single-line diagram. The network functions at a nominal frequency of 50 Hz, with loads acting as complex power sources that absorb electricity and generators acting as complex power sources that inject power into the system. Established methods for distribution network analysis are used to model the components of the power system. Synchronous generator characteristics with automatic voltage controls are used to model generators as sophisticated power sources that inject electricity into the system. With three-phase voltage-current measurement blocks, three-phase breakers for protection, and three-phase series resistance-inductance-capacitance load arrangements, the generators use three-phase programmable voltage sources. Bus bars can be categorized and modeled as either PQ buses (load buses with specified active and reactive power) or PV buses (generator buses with specified voltage magnitude and active power). Loads are implemented as PQ data-based lumped loads that represent the features provided in Tables 1 and are modeled as complicated power sources absorbing power.

Table 1: Onitsha Distribution Network Load Centre Specifications [9]

Bus Number	Bus Name	Active Load (MW)	Power Factor	Apparent Load (kVA)
1	Awada FDR 8 11Kv	7.0	0.935	7.487
2	Mgbemena 11kV	8.0	0.952	8.403
3	Okpoko 11Kv	5.0	0.891	5.612
4	G.R.A 11kV	5.0	0.973	5.139
5	Omoba 11kV	5.0	0.941	5.314
6	Minaj 11kV	2.0	0.934	2.141
7	Inland Town 11kV	5.0	0.954	5.241
8	Industrial Line Load	2.0	0.978	2.045
9	Primer 11kV	1.0	0.944	1.059
10	Whaft 11kV	0.1	0.997	0.100
11	Iyiowa 11kV	4.0	0.885	4.520
12	Iweka 11kV	4.0	0.897	4.459
13	Housing 11kV	3.0	0.902	3.326
14	Water Works 11kV	3.5	0.911	3.842

15	Uga 11kV	3.5	0.959	3.650
Bus Number	**Bus Name**	**Active Load (MW)**	**Power Factor**	**Apparent Load (kVA)**
16	Fegge 11kV	1.5	0.950	1.579
17	Bida 11kV	4.0	0.897	4.459
18	Market 11kV	5.5	0.919	5.985
19	Harbor 11kV	3.5	0.900	3.889
20	Golden Oil 33kV	2.6	0.950	2.737
21	E.Amobi 33kV	1.5	0.945	1.587
22	Interfact 11kV	3.0	0.942	3.185
23	G.C.M 11kV	0.1	0.950	0.105
24	Dozzy 11kV	2.0	0.905	2.210
25	PP1 11kV	1.0	0.931	1.074
26	IUNT 11kV	2.0	0.910	2.198
27	Ezeiweka 11Kv	6.0	0.920	6.522
28	Nwaziki 11Kv	6.0	0.952	6.303
29	Woliwo 11Kv	4.0	0.939	4.260

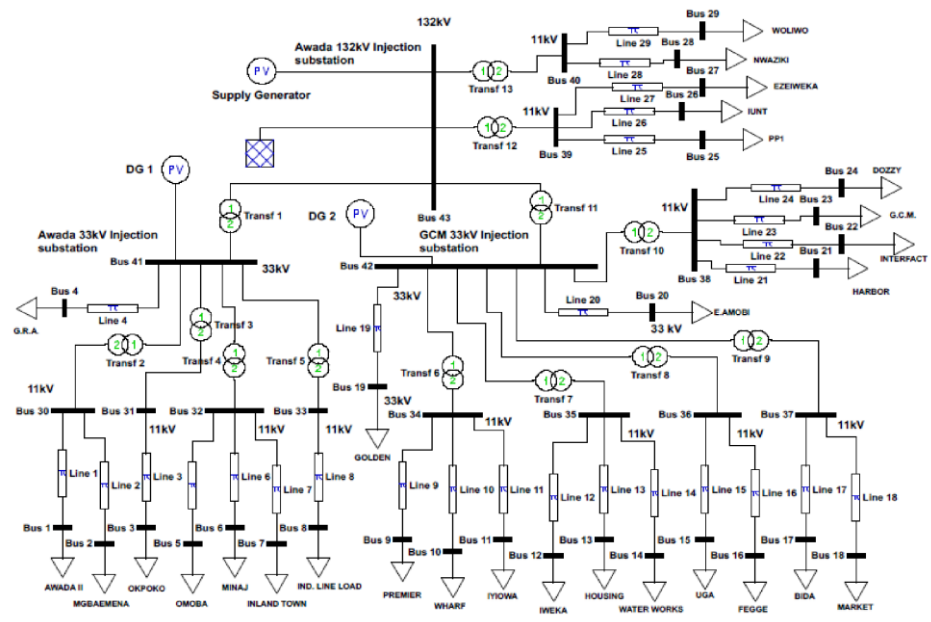

Figure 1: Single-line diagram of Onitsha 11kV distribution network system showing substations, transmission lines, and load centers [9]

3. Electric vehicle model

In order to capture the dynamics of charging and discharging, the electric vehicle battery is modeled as a regulated DC source with internal resistance on MATLAB. The battery terminal voltage relationship is expressed in Equation 1 [10]:

$$Vbat = VO - RintIbat \quad (1)$$

Where V_{bat} represents the terminal voltage, V_O denotes the open circuit voltage dependent on state of charge, R_{int} represents the internal resistance, and I_{bat} denotes the battery current. Equation 2 [11] describes the exponential voltage rise features of the battery charging process:

$$V(t) = V_{max}(1 - e^{-\frac{t}{RC}}) \quad (2)$$

where R stands for equivalent resistance in the charging path, C for capacitance, t for time, V(t) for voltage at time t, and Vmax for the electric car battery's final voltage. On the other hand, as shown in Equation 3 [11], battery draining displays exponential voltage decay:

$$V(t) = V_0 e^{-\frac{t}{RC}} \quad (3)$$

where V_0 is the initial voltage at the start of the discharge. Accurate modeling of the battery state of charge evolution during charging and discharging operations is made possible by these relationships. Bidirectional power electronic converters are necessary for grid integration with electric vehicles in order to provide both grid-to-vehicle and vehicle-to-grid charging and discharging. The converter system consists of a buck-boost converter that controls battery charging and discharging after a front-end active rectifier that converts alternating current grid electricity to direct current while maintaining a constant voltage across the direct current bus. Equation 4 [10] describes how the inverter step converts direct current to alternating current:

$$v_{abc} = MV_{dc}\sin(\omega t) \quad (4)$$

Where M represents the modulation index, V_{dc} denotes the direct current link voltage, and ω\omega ω represents grid angular frequency. Equation 5 implies that during charging operations, the buck converter lowers voltage [10]:

$$V_{out} = DV_{in} \qquad \text{where } 0 < D < 1 \quad (5)$$

Where D represents the duty cycle controlling output voltage reduction, V_{in} denotes input voltage, and V_{out} represents output voltage. The buck converter dynamics are governed by Equation 6 [10]:

$$\frac{dI_L}{dt} = \frac{V_{in} - V_{out}}{L}; \quad \frac{dV_{out}}{dt} = \frac{I_L - I_{load}}{C} \quad (6)$$

Where L represents inductance, C denotes capacitance, I_L represents inductor current, and I_{load} denotes load current. The boost converter increases voltage during discharging operations following Equation 7 [10]:

$$V_{out} = \frac{V_{in}}{1 - D} \quad \text{where } 0 < D < 1 \quad (7)$$

With dynamics expressed in Equation 8 [10]:

$$\frac{dI_L}{dt} = \frac{V_{in}}{L}; \quad \frac{dV_{out}}{dt} = \frac{I_L - I_{load}}{C} \quad (8)$$

The block diagram for electric car battery charging control is shown in Figure 2, where the pulse width modulation for charging activities is controlled by the positive current reference (I_{bat}^{ref}). The battery discharge control using negative current reference ($-I_{bat}^{ref}$) for vehicle-to-grid power injection is shown in Figure 3. Both implementations use current limiters to avoid excessive current flows, fuzzy logic control for intelligent adaptive regulation, and pulse width modulation to provide commands for active power (PWM1) and reactive power (PWM2).

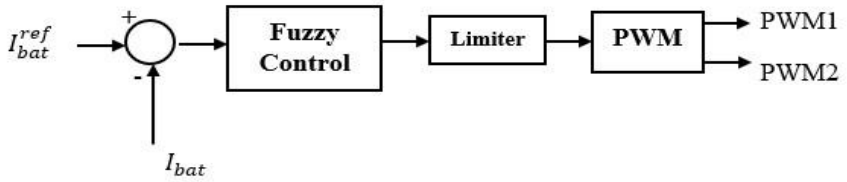

Figure 2: Block diagram of electric vehicle battery charging control system showing fuzzy controller, current reference, and pulse width modulation generation [12]

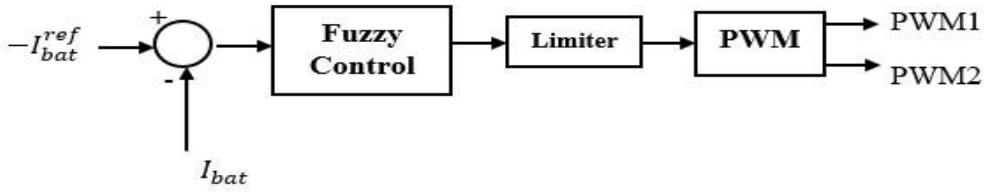

Figure 3: Block diagram of electric vehicle battery discharging control system for vehicle-to-grid operation [12]

4. Controller design

This section explained the MIMO fuzzy controller design.

4.1 Inputs & Outputs

i. Inputs: SOC (Low, Medium, High — trapmf/trimf), Time Remaining (Short, Medium, Long), Grid Frequency (Low, Nominal, High), Grid Voltage (Low, Nominal, High).
ii. Outputs: Charging Rate (Range [-1,1], 7 MFs defined as Fash discharging, Moderate discharging, Slow discharging, Ideal, Slow Charging, Moderate Charging, Fast Charging).
iii. Grid Stability Index: 3 MFs (Very Unstable, Unstable, Stable).

4.2 Membership details

The study input membership function coverage includes:

Input 1: State of charge (SOC) the range is between [0-100%] and the subsets are as follows:

i. Low (L): The membership function is trapmf the range is between [0, 0, 20, 40]
ii. Medium (M): The membership function is trimf the range is between [20, 50, 80]
iii. High (H): The membership function is trapmf the range is between [60, 80, 100, 100].
The SOC membership function graph for this coverage is as shown in Figure 4

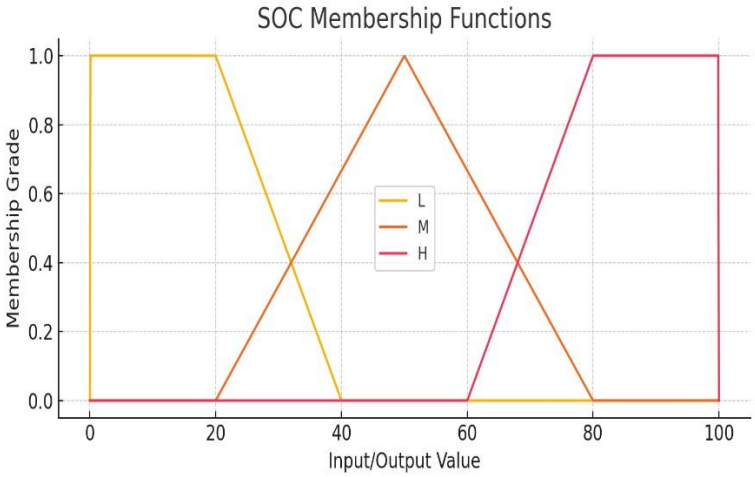

Figure 4: SOC Membership Functions

Input 2: Time Remaining (hrs) the range is between [0-24] and the subsets are as follows:

i. Short (S): The membership function is trapmf the range is between [0, 0, 4, 8]
ii. Medium (M): The membership function is trapmf the range is between [3, 11, 13, 21]
iii. Long (LO): The membership function is trapmf the range is between [16, 20, 24, 24].

The Time Remaining membership function graph for this coverage is as shown in Figure 5.

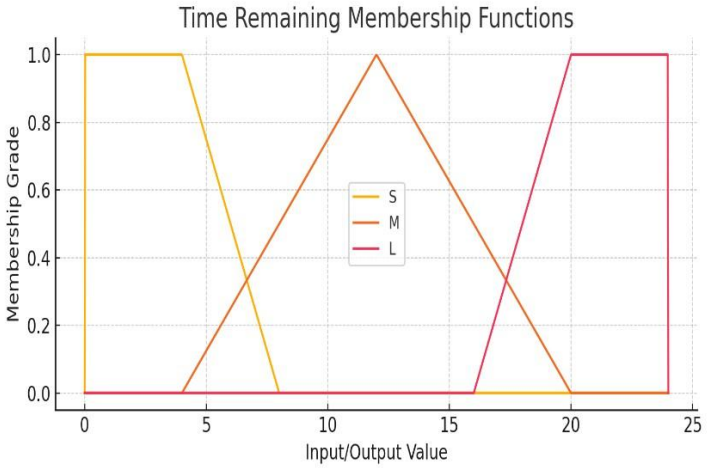

Figure 5: Time Remaining Membership Functions

Input 3: Frequency (Hz) the range is between [0-50] and the subsets are as follows:

i. Low (L): The membership function is trapmf the range is between [0, 0, 15, 30]
ii. Nominal (N): The membership function is trimf the range is between [25, 35, 40]
iii. High (H): The membership function is trapmf the range is between [38, 45, 50, 50]

The frequency membership function graph for this coverage is as shown in Figure 6.

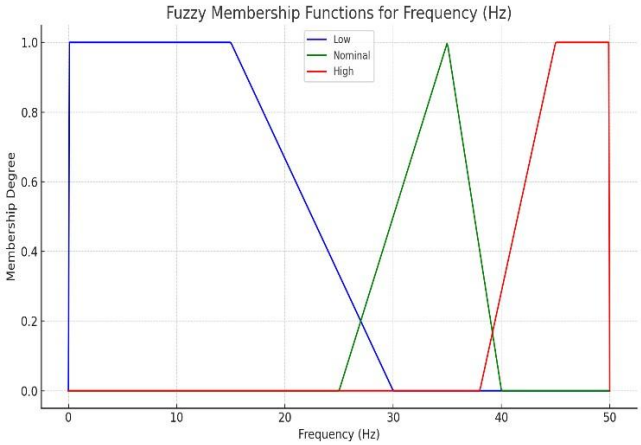

Figure 6: Frequency Membership Functions

Input 4: Voltage (V) the range is between [0-400] and the subsets are as follows:

i. Low (L): The membership function is trapmf the range is between [0, 0, 100, 200]
ii. Nominal (N): The membership function is trimf the range is between [190, 250, 300]
iii. High (H): The membership function is trapmf the range is between [290, 350, 400, 400].

The voltage membership function graph for this coverage is as shown in Figure 7.

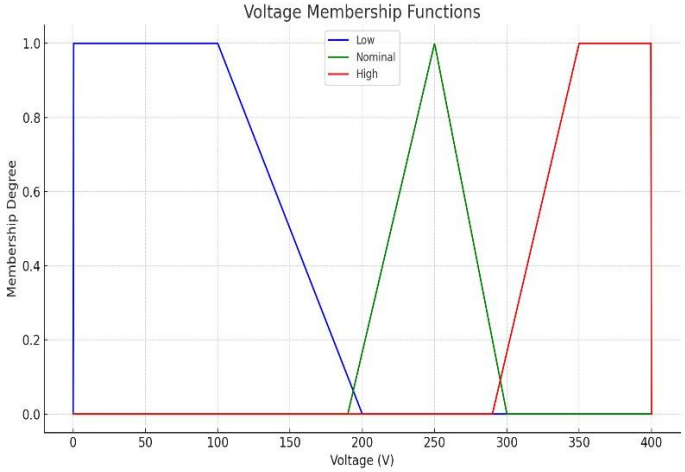

Figure 7: Voltage Membership Functions

The study output membership function coverage includes:

Output 1: Charging Rate the range is between [-1 to 1] and the subsets are as follows:

i. Fast discharging (FD): The membership function is trapmf the range is between [-1, -1, -0.8, -0.6]
ii. Moderate discharging (MD): The membership function is trimf the range is between [-0.8, -0.4, -0.2]
iii. Slow discharging (SD): The membership function is trimf the range is between [-0.4, -0.2, 0]
iv. Idle (I): The membership function is trimf the range is between [-0.1, 0, 0.1]
v. Slow charging (SC): The membership function is trimf the range is between [0, 0.2, 0.4]
vi. Moderate charging (MC): The membership function is trimf the range is between [0.2, 0.4, 0.6]

vii. Fast charging (FC): The membership function is trapmf the range is between [0.6, 0.8, 1, 1]. The charging rate membership function graph for this coverage is as shown in Figure 8.

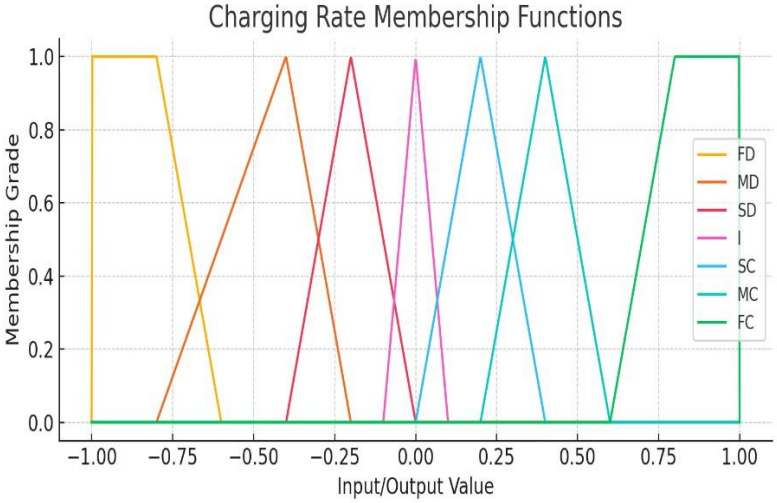

Figure 8: Charging Rate Membership Functions

Output 2: Grid Stability the range is between [0 to 1] and the subsets are as follows:

i. Very Unstable (VU): The membership function is trapmf the range is between [0, 0, 0.3, 0.4]

ii. Unstable (U): The membership function is trimf the range is between [0.3, 0.5, 0.7]

iii. Stable (S): The membership function is trapmf the range is between [0.6, 0.8, 1, 1]. The Grid stability membership function graph for this coverage is as shown in Figure 9.

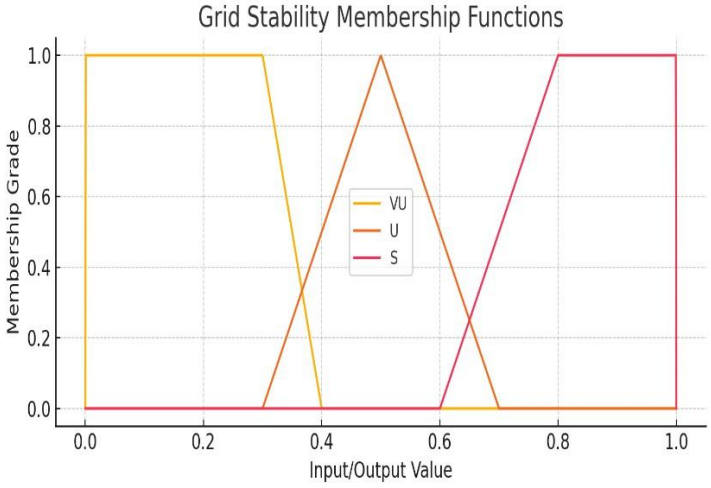

Figure 9: Grid Stability Membership Functions

4.3 Rule Base

Expert information regarding grid stability linkages and charging techniques is converted into formal if-then rules by the fuzzy rule base. Three SOC levels × three-time levels × three frequency levels × three voltage levels = 81 rules are used by the controller to cover every possible combination of input condition. The full rule-based structure is shown in Table 2.

Table 2: Complete Fuzzy Logic Rule Base (81 Rules)

Rule	SOC	TR	F	V	CR	GS
1	L	S	L	L	I	VU
2	L	S	L	N	I	VU
3	L	S	L	H	I	VU
4	L	S	N	L	I	VU
5	L	S	N	N	FC	S
6	L	S	N	H	FC	S
Rule	**SOC**	**TR**	**F**	**V**	**CR**	**GS**
7	L	S	H	L	I	VU
8	L	S	H	N	MC	U
9	L	S	H	H	MC	U
10	L	M	L	L	I	VU
11	L	M	L	N	I	VU
12	L	M	L	H	I	VU
13	L	M	N	L	I	VU
14	L	M	N	N	MC	S
15	L	M	N	H	MC	S
16	L	M	H	L	I	VU
17	L	M	H	N	SC	U
18	L	M	H	H	SC	U
19	L	L	L	L	I	VU
20	L	L	L	N	I	VU
21	L	L	L	H	I	VU
22	L	L	N	L	I	VU

23	L	L	N	N	SC	S
24	L	L	N	H	SC	S
25	L	L	H	L	I	VU
26	L	L	H	N	SC	U
27	L	L	H	H	SC	U
28	M	S	L	L	I	VU
29	M	S	L	N	I	VU
Rule	**SOC**	**TR**	**F**	**V**	**CR**	**GS**
30	M	S	L	H	I	VU
31	M	S	N	L	I	VU
32	M	S	N	N	MC	S
33	M	S	N	H	MC	S
34	M	S	H	L	I	VU
35	M	S	H	N	MC	U
36	M	S	H	H	MC	U
37	M	M	L	L	I	VU
38	M	M	L	N	I	VU
39	M	M	L	H	I	VU
40	M	M	N	L	I	VU
41	M	M	N	N	I	S
42	M	M	N	H	I	S
43	M	M	H	L	I	VU
44	M	M	H	N	SC	U
45	M	M	H	H	SC	U

46	M	L	L	L	I	VU
47	M	L	L	N	I	VU
48	M	L	L	H	I	VU
49	M	L	N	L	I	VU
50	M	L	N	N	SC	S
51	M	L	N	H	SC	S
52	M	L	H	L	I	VU
Rule	**SOC**	**TR**	**F**	**V**	**CR**	**GS**
53	M	L	H	N	SC	U
54	M	L	H	H	SC	U
55	H	S	L	L	FD	VU
56	H	S	L	N	FD	VU
57	H	S	L	H	FD	VU
58	H	S	N	L	FD	VU
59	H	S	N	N	MD	S
60	H	S	N	H	MD	S
61	H	S	H	L	FD	VU
62	H	S	H	N	MD	U
63	H	S	H	H	MD	U
64	H	M	L	L	MD	VU
65	H	M	L	N	MD	VU
66	H	M	L	H	MD	VU
67	H	M	N	L	MD	VU
68	H	M	N	N	SD	S
69	H	M	N	H	SD	S

70	H	M	H	L	MD	VU
71	H	M	H	N	SD	U
72	H	M	H	H	SD	U
73	H	L	L	L	MD	VU
74	H	L	L	N	MD	VU
75	H	L	L	H	MD	VU
Rule	**SOC**	**TR**	**F**	**V**	**CR**	**GS**
76	H	L	N	L	MD	VU
77	H	L	N	N	I	S
78	H	L	N	H	I	S
79	H	L	H	L	MD	VU
80	H	L	H	N	I	U
81	H	L	H	H	I	U

5. Performance evaluation

The performance evaluation metrics are addressed in this section.

5.1 Scenarios tested (5)

Five distinct charging and discharging scenarios that represent various operational settings are examined in the controller evaluation:

i. Scenario 1: When the state of charge is low, the departure time is brief, and the frequency and voltage are nominal, charging priority takes place. This scenario produces a fast charging rate command and a stable grid stability index by prioritizing rapid charging while preserving stable grid circumstances.

ii. Scenario 2: When departure time and condition of charge are medium and frequency and voltage are nominal, grid stability priority takes place. This scenario creates a stable grid stability index and idle charging rate command by balancing charging requirements against grid conditions.

iii. Scenario 3: When the condition of charge is medium, the departure time is brief, and the frequency and voltage are nominal, balanced charging and stability take place. This situation maximizes both goals, resulting in sustained grid stability and a reasonable charge rate.

iv. Scenario 4: When the state of charge is low, the departure time is short, but the frequency and voltage are low, grid stability becomes crucial. In this case, grid stability takes precedence over charging speed, resulting in an extremely unstable grid stability index and commands for idle or slow charging rates, which may cause vehicle-to-grid support.

v. Scenario 5: A high state of charge, a brief departure time, and low frequency and voltage all contribute to rapid discharge. In order to maintain grid stability, this scenario uses vehicle-to-grid discharge, which generates a fast discharging rate instruction while recognizing extremely unstable grid conditions.

5.2 Representative results

The developed MIMO fuzzy logic controller (four inputs, two outputs), a DISO fuzzy logic controller (two inputs, one output) that represents existing literature approaches [13], and a conventional PI controller [14]–[15] that represents traditional charging infrastructure were the three different control approaches that were assessed across five operating scenarios to determine relative performance. To allow for a fair comparison, every controller was tested using the same loading situations and network circumstances (Onitsha network). The thorough performance comparison for every scenario on the Onitsha network is shown in Table 3. Table 3 shows that the three controllers exhibit different performance patterns. In every situation, the MIMO fuzzy controller consistently produced the highest stability indices, which ranged from 0.174 in critical circumstances to 0.826-0.846 in stable settings. In the charging priority scenario (0.000, signifying total instability) and grid critical scenario (0.050), the DISO fuzzy controller demonstrated poorer stability indices. Depending on the situation, the PI controller's stability performance ranged from 0.030 to 0.750.

Table 3: Controller Performance Comparison Across All Scenarios on Onitsha network

Scenario	Controller	Charging Rate (A)	Stability Index	Frequency Deviation (Hz)
Charging Priority	MIMO Fuzzy	106.1	0.846	0.17
	DISO Fuzzy	101.2	0.000	0.20
	PI Controller	125.0	0.500	0.12
Grid Stability Priority	MIMO Fuzzy	~0	0.831	0.05
	DISO Fuzzy	0.0	0.600	0.08
	PI Controller	50.0	0.700	0.06
Balanced Charging	MIMO Fuzzy	50.0	0.826	0.10
	DISO Fuzzy	87.5	0.700	0.10
	PI Controller	75.0	0.750	0.09
Grid Critical	MIMO Fuzzy	~0	0.174	0.35
	DISO Fuzzy	106.1	0.050	0.40
	PI Controller	125.0	0.030	0.45
Rapid Discharging	MIMO Fuzzy	-109.3	0.174	0.35
	DISO Fuzzy	-102.7	0.100	0.38
	PI Controller	-125.0	0.050	0.42

Frequency deviation patterns typically show the MIMO controller's improved disturbance rejection. The PI controller achieved the lowest deviation (0.12 Hz) for charging priority due to its slower charging rate ramping, whereas the MIMO controller produced a deviation of 0.17 Hz as opposed to DISO's 0.20 Hz. However, under the critical grid situation, the MIMO controller's safe idle mode limited deviation to 0.35 Hz, whereas the DISO and PI controllers continued to function under severe grid stress, producing deviations of 0.40 Hz and 0.45 Hz, respectively. The different control philosophies are highlighted by the comparison of charge rates.

The PI controller maintains maximum rates (±125A) under all conditions, the MIMO controller adapts throughout a wider range (0-109A) including frequency and duration constraints, and the DISO controller modulates between 0-106A dependent on voltage and charge status. The ability of the MIMO controller to enter protective idle mode in grid-critical scenarios (charging rate ~0A) is a significant safety feature that the other approaches lack. The left panel of Figure 10 displays the grid stability index that each controller achieved in each of the five circumstances. The MIMO fuzzy controller (blue bars) continuously produces the highest stability indices (0.826-0.846) in scenarios 1-3, suggesting better stability preservation during normal operation.

All controllers exhibit low stability indices (0.03-0.174) in scenarios 4-5 (grid critical and rapid discharge), but the MIMO controller's higher values (0.174) reveal comparatively better performance even under extreme stress. The PI controller (yellow bars) has the most varied performance (0.030 to 0.750), while the DISO fuzzy controller (orange bars) displays intermediate performance with indices ranging from 0.000 to 0.700. Frequency deviation magnitudes are shown in the panel on the right. According to the pattern, in four out of five scenarios, the MIMO controller achieves the lowest or nearly the lowest deviations. The grid critical case is also noteworthy, in which the blind operation of the PI controller results in a deviation of 0.45 Hz, whereas the protective behavior of the MIMO controller limits variation to 0.35 Hz. By using intelligent control, this 0.10 Hz difference indicates a 22% decrease in frequency disturbance.

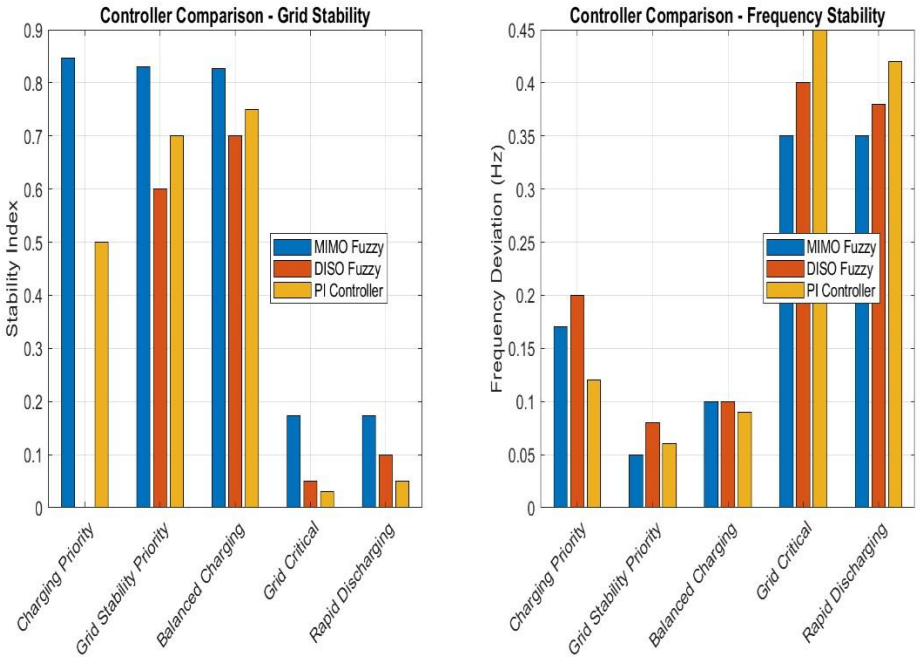

Figure 10: Controller Performance Comparison on Onitsha network- Grid Stability and Frequency Deviation

The results of every statistical test are compiled in Table 4. According to Table 4, the MIMO controller was statistically significant in two of the four pairwise comparisons: frequency deviation versus DISO control (p=0.0264) and stability index versus PI control (p=0.0259). Although the non-significant results for MIMO versus DISO stability (p=0.1280) and MIMO versus PI frequency (p=0.4293) show that controller performance advantages vary by metric and comparison, these results offer some statistical evidence of MIMO superiority.

Table 4: Statistical Hypothesis Test Results (α=0.05)

Test	**Comparison**	**Metric**	**p-Value**	**Significant?**	**Conclusion**
Paired t-test	MIMO vs DISO	Stability Index	0.1280	No	No significant difference

Paired t-test	MIMO vs PI	Stability Index	0.0259	Yes*	MIMO significantly better
Paired t-test	MIMO vs DISO	Frequency Deviation	0.0264	Yes*	MIMO significantly better
Paired t-test	MIMO vs PI	Frequency Deviation	0.4293	No	No significant difference
One-way ANOVA	All three	Stability Index	0.4651	No	No overall difference
One-way ANOVA	All three	Frequency Deviation	0.9503	No	No overall difference

*Statistically significant at α=0.05 level

The statistical test findings are visualized in Figure 11 by comparing the p-value to the significance threshold. Figure 11 displays the p-values for each of the six statistical tests as bar heights, with a red dashed line representing the α=0.05 criteria. Red asterisks indicate that tests 2 and 3 (MIMO vs. PI stability and MIMO vs. DISO frequency) with p-values below this line are deemed significant. Because their p-values are greater than the cutoff, tests 1, 4, 5, and 6 do not achieve significance. The ANOVA tests (5 and 6) show p-values near 1.0 when all three controllers are considered simultaneously, suggesting no appreciable changes.

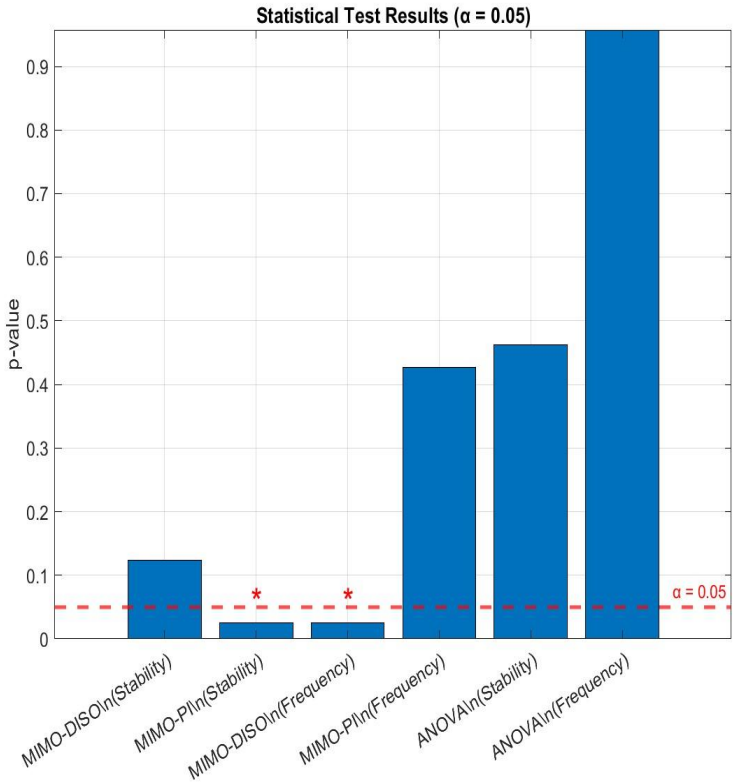

Figure 11: Statistical Test Results - p-Values Relative to α=0.05 Threshold

The uneven statistical results reflect the inherent difficulties of evaluating controller performance with limited sample sets (five situations). Power analysis indicates that in order to detect the observed effect sizes with 80% power, it would require approximately 8–12 scenarios for stability index comparisons and 15–20 scenarios for frequency deviation comparisons. Despite the small sample size, the significant results show that the benefits of the MIMO controller are robust in some pairwise comparisons.

6. Conclusion

In order to simultaneously optimize EV charging behavior and grid stability inside the Onitsha distribution network, this study successfully developed and implemented a MIMO Mamdani fuzzy logic controller. The controller outperformed conventional PI and DISO fuzzy controllers in terms of flexibility and responsiveness by combining SOC, time remaining, voltage, and frequency into a single control framework. When grid circumstances worsened, the controller could transition between fast charging, moderated charge, idle mode, and V2G support thanks to the 81-rule framework's ability to make intelligent decisions under a variety of operating scenarios. The suggested controller continuously produced the greatest stability indices, decreased frequency deviations, and implemented protective actions throughout extremely unstable grid periods, according to performance evaluations across five illustrative situations. The MIMO controller struck a compromise between user charging requirements and system security, whereas DISO controllers lacked multi-objective awareness and PI controllers tended to overcharge and disrupt the network. Its benefits were further confirmed by statistical tests, which showed notable gains in stability and frequency deviation measures. All things considered, the controller improves grid dependability, facilitates safe EV adoption, and tackles issues related to real-time charging coordination in inadequate distribution systems. To further improve grid EV interactions, future research should investigate hybrid intelligent control systems, increase the number of test scenarios, and take renewable energy fluctuation into account.

Acknowledgments

I am incredibly appreciative to Almighty God for giving me the fortitude, discernment, health, and tenacity I needed to complete this study project.
My profound gratitude is extended to my supervisor, Professor Paul Kehinde Olulope, and Professor Marion Adebiyi, whose advice, support, and wise counsel were crucial to the accomplishment of my thesis. I sincerely appreciate all of the time and energy that went into evaluating and improving my work.
I also want to express my gratitude to all of the academic and non-academic staff at Landmark University's Department of Electrical and Information Engineering for creating a supportive learning atmosphere and helping me with my studies. A special thank you to my parents, Mr. and Mrs. Onyemenam; my siblings, Joseph, Joshua, Joy, Joel, and Jerimiah; and my friends, Engineer Victor Ejenam, Engineer Abolarinwa, Dr. Daniel, and Dr. Michael Arowolo, for their unflinching love, support, and encouragement, particularly during difficult times. Finally, I would like to express my gratitude to everyone who helped make this research a success. We will always be grateful for your help and efforts.
I'm grateful to everyone.

References

[1] Yang, H., Yang, S., Xu, Y., Cao, E., Lai, M., & Dong, Z. (2015). Electric vehicle route optimization considering time-of-use electricity price by learnable partheno-genetic algorithm. *IEEE Transactions on Smart Grid*, *6*(2), 657–666. https://doi.org/10.1109/TSG.2014.2382684

[2] Qian, K., Zhou, C., Allan, M., & Yuan, Y. (2011). Modeling of load demand due to EV battery charging in distribution systems. IEEE Transactions on Power Systems, 26(2), 802–810. https://doi.org/10.1109/TPWRS.2010.2057456

[3] J. Onyemenam, P. Olulope, M. Adebiyi, O. Akinoshun, V. Ejenam, I. Onyemenam & L. Onyemenam. (2025). Negative impacts of electric vehicle integration on the grid: A review. *NIPES-Journal of Science and Technology, Research Vol. 7(2), Special Issue: Landmark University International Conference SEB4SDG 2025, pp. 2821–2827*

[4] Tang, Q., Xie, M., Yang, K., Luo, Y., Zhou, D., & Song, Y. (2019). A decision function based smart charging and discharging strategy for electric vehicle in smart grid. Mobile Networks and Applications, 24(5), 1722–1731. https://doi.org/10.1007/s11036-018-1049-4

[5] Vastardis, N., & Yang, K. (2013). Mobile social networks: Architectures, social properties, and key research challenges. IEEE Communications Surveys and Tutorials, 15(3), 1355–1371. https://doi.org/10.1109/SURV.2012.060912.00108

[6] Samuel Onodjohwo, Bankole Adebanji, Folashade Ariba, Emmanuel Taiwo Fasina, Isaac Onimisi Yusuf, and Adenike Josephine (2024). " Need for Network Reconfiguration in Nigerian distribution systems: A Review. *International conference on science, Engineering and Business for driving sustainable developments goals (SEB4SDG), 2024.*

[7] Kumar, R. R., & Alok, K. (2020). Adoption of electric vehicle: A literature review and prospects for sustainability. Journal of Cleaner Production, 253, Article 119911. https://doi.org/10.1016/j.jclepro.2019.119911

[8] Adekunle Kolawole, Olayinka Oluwole Agboola, Peter Pelumi Ikubanni, Olakunle Ganiyu Raji and Christian Okechukwu Osueke (2019). "Reliability and power loss analysis: A case study of a power plant in Nigeria". Cogent Engineering, 6(1), 2019.

[9] Enugu Electricity Distribution Company (EEDC). (2020). Onitsha work center diary 2020.

[10] Nayak, P. S. R., Kamalapathi, K., Laxman, N., & Tyagi, V. K. (2021, January). Design and simulation of buckboost type dual input DC-DC converter for battery charging application in electric vehicle. In 2021 International Conference on Sustainable Energy and Future Electric Transportation (SEFET) (pp. 1–6). IEEE. https://doi.org/10.1109/SEFET48154.2021.9375739

[11] Parvini, Y. (2016). Modeling, hybridization, and optimal charging of electrical energy storage systems [Doctoral dissertation, Clemson University]. TigerPrints.

[12] Siddanthi Abhilash, K.Giri Babu, J.Kartigeyan (2024). Fuzzy logic controller based G2V & V2G Technologies for Three Phase Bidirectional Electric Vehicle Battery Charger. Industrial Engineering Journal, ISSN: 0970-2555, Volume: 53, Issue 7, July: 2024.

[13] Alshogeathri, A. M. A. (2016). Vehicle-to-grid (V2G) integration with the power grid using a fuzzy logic controller [Doctoral dissertation, Kansas State University]. K-State Research Exchange.

[14] Karuppiah, M., Dineshkumar, P., & Karthikumar, K. (2020, December). Design a electric vehicle charger based sepic topology with PI controller. In 2020 IEEE International Conference on Advances and Developments in Electrical and Electronics Engineering (ICADEE) (pp. 1-5). IEEE.

[15] Sayed, K., & Gabbar, H. A. (2016). Electric vehicle to power grid integration using three-phase three-level AC/DC converter and PI-fuzzy controller. Energies, 9(7), 532.